

Localization of Sphingomyelin in Cholesterol Domains by Imaging Mass Spectrometry

Carolyn M. McQuaw,[†] Leiliang Zheng,[‡] Andrew G. Ewing,[‡] and Nicholas Winograd^{*‡}

Vollum Institute and Department of Molecular Microbiology & Immunology, Oregon Health and Science University, Portland, Oregon 97201-3098, and Department of Chemistry, The Pennsylvania State University, 104 Chemistry Building, University Park, Pennsylvania 16802

Received November 6, 2006. In Final Form: February 15, 2007

The location of each lipid in a palmitoylcholine/18:0 sphingomyelin/cholesterol monolayer system is laterally resolved using imaging time-of-flight secondary ion mass spectrometry (TOF-SIMS) without the necessity of adding fluorescent labels. This system of coexisting immiscible liquid phases shows cholesterol domains with sizes and shapes comparable to those in the fluorescence microscopy literature. The results show that SM localizes with cholesterol and that palmitoylcholine is excluded. Moreover, the segregation is not complete, and there is a small amount of both phospholipids distributed throughout.

Introduction

Upon the basis of the detergent-resistant fraction of cellular membranes, the content of lipid rafts includes sphingomyelin and cholesterol.¹ Both cholesterol and sphingomyelin have been hypothesized to be essential for lipid raft formation in the cellular membrane.² Also, a recent study of the native HIV membrane lipidome provides strong evidence for the existence of lipid rafts in living cells.³ Currently, a substantial body of research is focused on elucidating the interactions between cholesterol and sphingomyelin (ref 4 and references therein). Many methods have been used to investigate sphingomyelin–cholesterol interactions, including nuclear magnetic resonance spectroscopy (NMR)⁵ and fluorescence microscopy.^{4,6–13} To obtain images, fluorescence microscopy is the most common technique for visualizing lipid miscibility; however, it requires the addition of fluorescent labels. The degree of influence that the added fluorophores have on domain formation is still in question, but recently Cruz et al. found that trace amounts (<1 mol %) of this probe perturb the morphology of micro- and nanodomains of dipalmitoylphosphatidylcholine monolayers.¹⁴

One technique that is capable of direct chemical imaging of lipid domains is secondary ion mass spectrometry (SIMS).^{15–23}

In this technique, a focused ion beam is used to desorb secondary ions from the sample, and then the beam is moved across the surface and mass spectra are acquired at each spot on the surface. Using characteristic mass values, the lateral distribution of the individual chemical components are revealed.²⁴ There are two major approaches depending upon the fluence of the primary ion. With static SIMS, a pulsed primary ion beam is used, and the mass spectrum is measured before a significant part of the surface layer has been chemically modified and sputtered away. The low dose of the primary ion allows for high surface sensitivity and molecular information being obtained from the sample without chemical labeling. With dynamic SIMS, a continuous primary ion beam bombards the sample, which leads to sputtering of atoms from the surface. Dynamic SIMS is capable of elemental and isotope analysis and has higher lateral resolution for SIMS imaging. However, isotope labeling is usually required to differentiate molecular species in the sample system. Here we present static time-of-flight (TOF) SIMS studies on monolayers of palmitoylcholine (POPC)/18:0 sphingomyelin (SM)/cholesterol (CH). Without the use of chemical labels, we find that the ternary mixture of 30:47:23 POPC/18:0 SM/CH produces coexisting liquid phases in which SM is predominantly found within the CH-rich phase and the POPC is predominantly excluded. The location of SM is elucidated without the incorporation of any added labels. Also, TOF-SIMS shows clearly that the lipids do not entirely segregate from one another and illustrates the complexity of lipid interactions.

* Corresponding author. E-mail: nxw@psu.edu.

[†] Oregon Health and Science University.

[‡] The Pennsylvania State University.

(1) Simons, K.; Ikonen, E. *Nature* **1997**, *387*, 569–572.

(2) Brown, D. A.; Rose, J. K. *Cell* **1992**, *68*, 533–544.

(3) Brugger, B.; Blass, B.; Haberkant, P.; Leibrecht, I.; Wieland, F. T.; Krausslich, H. *Proc. Natl. Acad. Sci. U.S.A.* **2006**, *103*, 2641–2646.

(4) Holopainen, J. M.; Metso, A. J.; Mattila, J. P.; Jutila, A.; Kinnunen, P. K. *J. Biophys. J.* **2004**, *86*, 1510–1520.

(5) Eppard, R. M.; Eppard, R. F. *Chem. Phys. Lipids* **2004**, *132*, 37–46.

(6) Slotte, J. P. *Biochim. Biophys. Acta* **1995**, *1235*, 419–427.

(7) Dietrich, C.; Bagatolli, L. A.; Volovyk, Z. N.; Thompson, N. L.; Levi, M.; Jacobson, K.; Gratton, E. *Biophys. J.* **2001**, *80*, 1417–1428.

(8) Veatch, S. L.; Keller, S. L. *Phys. Rev. Lett.* **2002**, *89*, 268101–268104.

(9) de Almeida, R. F. M.; Fedorov, A.; Prieto, M. *Biophys. J.* **2003**, *85*, 2406–2416.

(10) McConnell, H. M.; Radhakrishnan, A. *Biochim. Biophys. Acta* **2003**, *1610*, 159–173.

(11) Crane, J. M.; Tamm, L. K. *Biophys. J.* **2004**, *86*, 2965–2979.

(12) Stottrup, B. L.; Stevens, D. S.; Keller, S. L. *Biophys. J.* **2005**, *88*, 269–276.

(13) Veatch, S. L.; Keller, S. L. *Phys. Rev. Lett.* **2005**, *94*, 148101–148104.

(14) Cruz, A.; Vazquez, L.; Velez, M.; Perez-Gil, J. *Langmuir* **2005**, *21*, 5349–5355.

(15) Biesinger, M. C.; Paegegaey, P.-Y.; McIntyre, N. S.; Harbottle, R. R.; Petersen, N. O. *Anal. Chem.* **2002**, *74*, 5711–5716.

(16) Bourdos, N.; Kollmer, F.; Benninghoven, A.; Ross, M.; Sieber, M.; Galla, H. J. *Biophys. J.* **2000**, *79*, 357–369.

(17) Harbottle, R. R.; Nag, K.; McIntyre, N. S.; Possmayer, F.; Petersen, N. O. *Langmuir* **2003**, *19*, 3698–3704.

(18) Kraft, M. L.; Weber, P. K.; Longo, M. L.; Hutcheon, I. D.; Boxer, S. G. *Science* **2006**, *313*, 1948–1951.

(19) Marxer, C. G.; Kraft, M. L.; Weber, P. K.; Hutcheon, I. D.; Boxer, S. G. *Biophys. J.* **2005**, *88*, 2965–2975.

(20) McQuaw, C. M.; Sostarecz, A. G.; Zheng, L.; Ewing, A. G.; Winograd, N. *Langmuir* **2005**, *21*, 807–813.

(21) McQuaw, C. M.; Zheng, L.; Ewing, A. G.; Winograd, N. *Appl. Surf. Sci.* **2006**, *252*, 6716–6718.

(22) Ross, M.; Steinem, C.; Galla, H.-J.; Janshoff, A. *Langmuir* **2001**, *17*, 2437–2445.

(23) Sostarecz, A. G.; McQuaw, C. M.; Ewing, A. G.; Winograd, N. *J. Am. Chem. Soc.* **2004**, *126*, 13882–13883.

(24) Henry, C. M. *Chem. Eng. News* **2004**, *82*, 33–35.

64

Materials and Methods

65 For lipid monolayer characterization by imaging TOF-SIMS,
 66 monolayers at the air–water interface were deposited vertically onto
 67 solid substrates via the Langmuir–Blodgett (LB) technique. Similar
 68 methods have also been utilized for analyses of lipid monolayers by
 69 atomic force microscopy,^{25,26} and supported LB films have been
 70 shown to maintain the same lateral distribution of lipids observed
 71 at the air–water interface.^{16,17} Although cellular membranes exist
 72 at higher pressures and temperatures, lower pressures are necessary
 73 to study lipid miscibility¹⁰ in the mixtures. To identify the contents
 74 of coexisting phases in our lipid monolayer, we have selected 7
 75 mN/m to ensure the existence of multiple phases in our system
 76 because fluorescence microscopy data is already available at similar
 77 pressures¹² for direct comparison. Also, recent studies suggest that
 78 the more relevant parameter to consider when comparing lipid
 79 monolayers to cellular membranes is the molecular density.¹² The
 80 molecular area of our ternary mixture at lower pressure is considerably
 81 closer to the molecular area per lipid of an erythrocyte membrane
 82 ($\sim 40 \text{ \AA}^2$ for the outer leaflet²⁷ and $\sim 60 \text{ \AA}^2$ for the inner leaflet²⁸)
 83 than that at very high pressure. The materials, substrate preparation,
 84 monolayer preparation and deposition, and TOF-SIMS characteriza-
 85 tion are briefly detailed here. All steps were completed at room
 86 temperature ($23 \pm 2 \text{ }^\circ\text{C}$).

87 **Materials.** POPC, CH (both from Avanti Polar Lipids, Inc.,
 88 Alabaster, AL), 18:0 SM (Matreya LLC, Pleasant Gap, PA), 16-
 89 mercaptohexadecanoic acid (Sigma-Aldrich, St. Louis, MO), 2-pro-
 90 panol, methanol, and chloroform were used without further
 91 purification. A Nanopure Diamond Life Science ultrapure water
 92 system (Barnstead International, Dubuque, IA) was used to purify
 93 the water used in the production of all monolayers (resistivity of
 94 $18.2 \text{ M}\Omega \text{ cm}$).

95 **Substrate Preparation.** Substrates were 16-mercaptohexade-
 96 canoic acid self-assembled monolayers (SAMs) on gold. The gold
 97 was deposited onto single-crystal (100) silicon wafers that were first
 98 cleaned via piranha etch (3:1 $\text{H}_2\text{SO}_4/\text{H}_2\text{O}_2$) to ensure a uniform SiO_2
 99 surface. (*Extreme caution must be exercised when using piranha*
 100 *etch. An explosion-proof hood should be used.*) The silicon substrates
 101 were deposited with chromium followed by gold as described by
 102 Fisher et al.²⁹ For the formation of the SAMs onto gold, a 1 mM
 103 solution of 16-mercaptohexadecanoic acid in 2-propanol was used.
 104 Gold deposition, SAM self-assembly, and LB film deposition were
 105 confirmed with a single-wavelength (632.8 nm, 1 mm spot size, 70°
 106 angle of incidence) Stokes ellipsometer (Gaertner Scientific Cor-
 107 poration, Skokie, IL; model LSE). SAMs on gold substrates were
 108 used because these provide higher positive ion SIMS signals of lipid
 109 monolayers than do silicon substrates³⁰ and they are also easily
 110 reproducible uniformly hydrophilic substrates necessary for our lipid
 111 monolayer deposition method.

112 **Monolayer Preparation, Isotherm Analysis, and Sample**
 113 **Deposition.** A Kibron μ Trough S-LB (Helsinki, Finland) was used
 114 for isotherm acquisition, LB film preparation, and deposition. The
 115 subphase was $\sim 65 \text{ mL}$ of purified water. All lipid solutions were
 116 dissolved in 9:1 chloroform/methanol. At least 15 min was allotted
 117 for film equilibration before compression to guarantee complete
 118 solvent evaporation. The surface pressure was measured with a
 119 Wilhelmy wire interfaced to a personal computer. Uniform com-
 120 pression ($7 \text{ \AA}^2/\text{molecule}/\text{min}$) of the lipid monolayer was ensured
 121 through computer control of the trough barriers, and this also allowed
 122 for constant pressure feedback during deposition. The lipid films

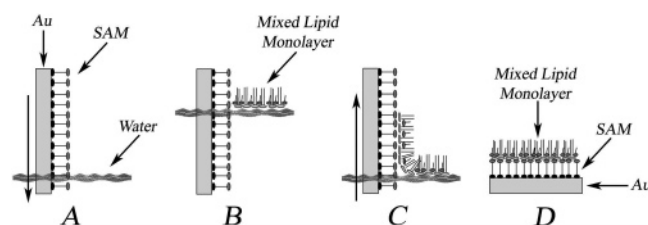


Figure 1. Side view of the vertical deposition of a mixed lipid monolayer onto a substrate. Sample preparation is detailed in the Materials and Methods section. (A) A 16-mercaptohexadecanoic acid self-assembled monolayer (SAM) on a gold (Au) substrate is inserted vertically through the water surface. (B) A mixed lipid monolayer is applied to the water surface and compressed to the desired surface pressure. (C) The substrate is lifted vertically through the water surface, and the mixed lipid monolayer adheres. (D) Schematic representation of the final sample.

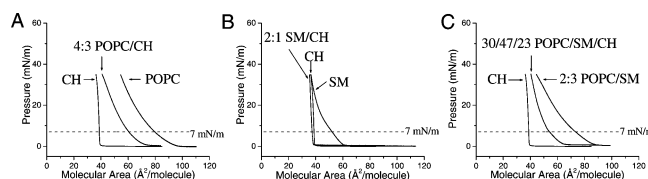


Figure 2. Pressure–area isotherms of mixtures containing POPC, CH, and 18:0 SM. (A) CH, POPC, and 4:3 POPC/CH. (B) CH, SM, and 2:1 SM/CH. (C) CH, 2:3 POPC/SM, and 30:47:23 POPC/SM/CH. The dotted line in each demarks a pressure of 7 mN/m.

were each deposited vertically onto SAM substrates at 7 mN/m upon first compression, resulting in a tails-up lipid configuration (Figure 1).

To quantify the influence of CH on POPC and SM, the molecular area of an ideal mixture (A_{ideal}) at 7 mN/m is compared to the actual molecular area observed (A_{actual}). A_{ideal} is the molecular area expected for a noninteracting, immiscible mixture.³¹ A_{ideal} is calculated by the following equation

$$A_{\text{ideal}} = X_1 A_1 + (1 - X_1) A_2 \quad (1)$$

where X_1 is the mole fraction of component 1, A_1 is the molecular area of pure component 1 at 7 mN/m, and A_2 is the molecular area of pure component 2 at 7 mN/m. Using A_{ideal} and A_{actual} , the condensing effect is quantified by determining the percent difference in the two molecular areas by the following equation:

$$\text{percent difference (\%)} = \frac{100\% \times (A_{\text{actual}} - A_{\text{ideal}})}{A_{\text{ideal}}} \quad (2)$$

Instrumentation. An imaging TOF-SIMS equipped with a 15 keV Ga^+ liquid metal ion gun was used to obtain mass spectrometric data. The mass spectrometer is described in detail by Braun et al.³² Spectra were acquired without the need for charge compensation and with an ion dose no greater than 10^{12} ions/ cm^2 . The ion beam diameter is $\sim 100 \text{ nm}$; however, for the data presented here, the pixel size ($\sim 1 \mu\text{m}^2$) is dictated by the field of view and the number of pixels. Each scan takes less than 30 s. Total ion images (256 pixels \times 256 pixels) were obtained by rastering the ion beam across the surface and taking a mass spectrum at each pixel. For the lipid molecular ion maps, the intensities of the individual lipid-specific ions (i.e., m/z 369 and 385 for CH) were summed at each pixel and then converted to a 64 pixel \times 64 pixel image by summing the intensities of surrounding pixels. Summing pixels is reasonable because the chemically resolved lipid domains were larger than 4 pixels \times 4 pixels.

(25) Yuan, C.; Johnston, L. J. *Biophys. J.* **2002**, *82*, 2526–2535.

(26) Lawrence, J. C.; Saslowsky, D. E.; Edwardson, J. M.; Henderson, R. M. *Biophys. J.* **2003**, *84*, 1827–1832.

(27) Van Deenen, L. L. M.; De Gier, J. In *The Red Blood Cell*; Surgenor, D. M., Ed.; Academic Press: New York, 1974; p 147.

(28) Marsh, D. *CRC Handbook of Lipid Bilayers*; CRC Press: Boca Raton, FL, 1990.

(29) Fisher, G. L.; Hooper, A. E.; Opila, R. L.; Allara, D. L.; Winograd, N. *J. Phys. Chem. B* **2000**, *104*, 3267–3273.

(30) Sostarecz, A. G.; Cannon, D. M., Jr.; McQuaw, C. M.; Sun, S.; Ewing, A. G.; Winograd, N. *Langmuir* **2004**, *20*, 4926–4932.

(31) Cadenhead, D. A.; Müller-Landau, F. J. *Colloid Interface Sci.* **1980**, *78*, 269–270.

(32) Braun, R. M.; Blenkinsopp, P.; Mullock, S. J.; Corlett, C.; Willey, K. F.; Vickerman, J. C.; Winograd, N. *Rapid Commun. Mass Spectrom.* **1998**, *12*, 1246–1252.

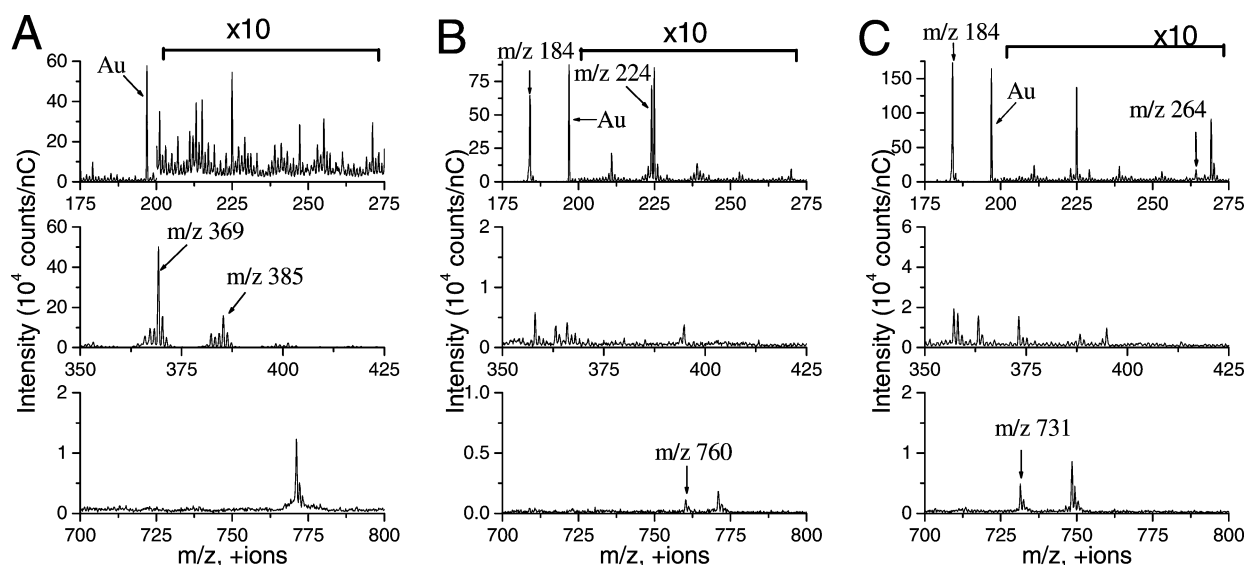


Figure 3. Mass spectra and significant +SIMS fragments of the pure lipids: (A) CH, (B) POPC, and (C) 18:0 SM. The characteristic ions are the POPC headgroup fragment $[C_8H_{19}NPO_4]^+$ at m/z 224, SM backbone fragment $[C_{17}H_{30}ON]^+$ at m/z 264, CH fragments $[M - OH]^+$ at m/z 369 and $[M - H]^+$ at m/z 385, 18:0 SM protonated molecular ion $[M + H]^+$ at m/z 731, and POPC protonated molecular ion $[M + H]^+$ at m/z 760. Phosphocholine $[C_5H_{15}NPO_4]^+$ at m/z 184) results from both POPC and SM. The intensity within m/z 200–275 has been multiplied by a factor of 10. The total ion dose was less than 10^{12} ion/cm² for each.

Table 1. Actual Average Molecular Area Observed at 7 mN/m (Using an Average of at Least Three Isotherms) and the Calculated Ideal Average Molecular Area of Each of the Mixtures as Well as the Percent Difference between the Two Areas for Each of the Mixtures

| sample | actual area (Å ² /molecule) | ideal area (Å ² /molecule) | percent difference (%) |
|-------------------------|--|---------------------------------------|------------------------|
| POPC | 82 ± 2.7 | | |
| 18:0 sphingomyelin (SM) | 53 ± 1.8 | | |
| cholesterol (CH) | 39 ± 1.3 | | |
| 2:3 POPC/SM | 70 ± 3.5 | 65 | 9 |
| 4:3 POPC/CH | 57 ± 6.3 | 63 | -8 |
| 2:1 SM/CH | 37 ± 0.2 | 48 | -20 |
| 2:3 POPC/SM + 23% CH | | 63 | -20 |
| 4:3 POPC/CH + 47% SM | 53 ± 3.3 | 55 | -5 |
| 2:1 SM/CH + 30% POPC | | 51 | 4 |

Results and Discussion

The lipids under analysis in this study are CH, POPC, and 18:0 SM. A saturated SM was selected because it is biologically more abundant than unsaturated SM.⁹ Similarly, an unsaturated phosphatidylcholine glycolipid was selected because they are more prevalent than saturated phosphatidylcholine glycolipids in the cellular membrane.⁹ These specific phospholipids were also chosen because fluorescence microscopy studies of similar monolayer mixtures have recently been presented in the literature.¹² This mixture contains a saturated lipid (SM), an unsaturated lipid (POPC), and CH and is known to produce immiscible liquid phases in both monolayers and bilayers.^{8,12,13} Herein, we illustrate TOF-SIMS as a viable resource for chemically resolving the lateral distribution of immiscible lipid mixtures and thus broadening the resources available for investigating lipid interactions.

Cholesterol Condenses a 2:3 POPC/18:0 Sphingomyelin Mixture. Pressure–area isotherms for each of the pure lipids, the binary mixtures, and the ternary mixture are presented in Figure 2. The actual and ideal molecular areas and the percent difference between the two are presented in Table 1. Isothermal data for the pure lipids are similar to literature values (i.e., for

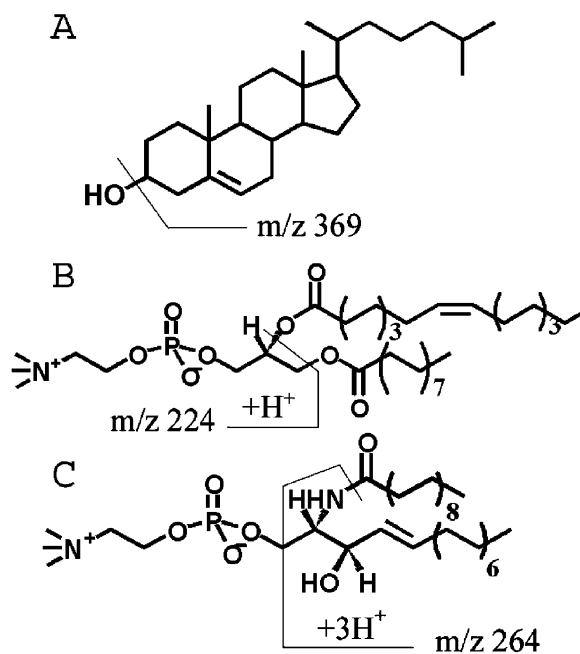


Figure 4. Molecular structures of (A) cholesterol (CH), (B) POPC, and (C) 18:0 SM with +SIMS fragment ions labeled. CH has two main fragments: $[M - H]^+$ at m/z 385 and $[M - OH]^+$ at m/z 369. POPC has two main fragments: $[M + H]^+$ at m/z 760 and $[C_8H_{19}NPO_4]^+$ at m/z 224. SM has two main fragments: $[M + H]^+$ at m/z 731 and $[C_{17}H_{30}ON]^+$ at m/z 264.

CH,²³ SM,³³ and POPC³⁴). It is clear that CH has a condensing 174 effect on both POPC (Figure 2A) and 18:0 SM (Figure 2B). The 175 2:1 SM/CH mixture has a molecular area that is nearly equal to 176 that of pure CH at 7 mN/m and is -20% different from ideal. 177 However, POPC has a much higher molecular area than 18:0 SM 178 at 7 mN/m and a smaller CH condensing effect (percent difference 179 of -8%). These results are similar to literature values (i.e., for 180

(33) Vaknin, D.; Kelley, M. S.; Ocko, B. M. *J. Chem. Phys.* **2001**, *115*, 7697–7704.

(34) Smaby, J. M.; Brockman, H. L.; Brown, R. E. *Biochemistry* **1994**, *33*, 9135–9142.

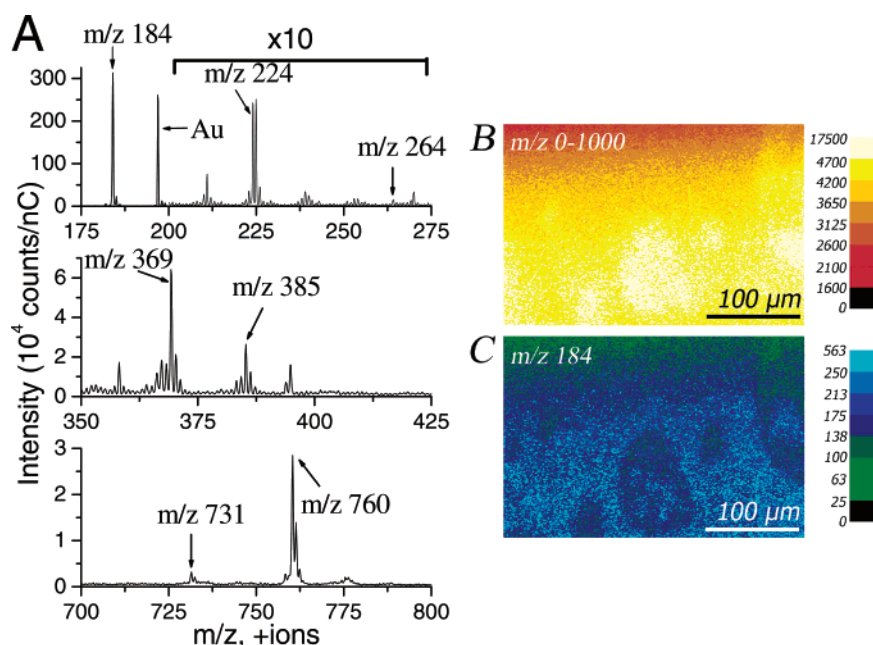


Figure 5. (A) Mass spectra with significant +SIMS fragments labeled for the ternary mixture 30:47:23 POPC/18:0 SM/CH. The characteristic ions are POPC headgroup fragment $[C_8H_{19}NPO_4]^+$ at m/z 224, SM backbone fragment $[C_{17}H_{30}ON]^+$ at m/z 264, cholesterol fragments $[M - OH]^+$ at m/z 369 and $[M - H]^+$ at m/z 385, 18:0 SM protonated molecular ion $[M + H]^+$ at m/z 731, and POPC protonated molecular ion $[M + H]^+$ at m/z 760. Phosphocholine $[C_5H_{15}NPO_4]^+$ at m/z 184) results from both POPC and SM. The intensity within m/z 200–275 has been multiplied by a factor of 10. The total ion dose was less than 10^{12} ion/cm². (B) Total ion image and (C) phosphocholine ion image ($[C_5H_{15}NPO_4]^+$ at m/z 184). Images are 256 pixels \times 256 pixels with the scale bar representing 100 μ m, ion intensity scales in counts/nC, and a total ion dose of less than 10^{12} ion/cm².

181 POPC/CH³⁴ and SM/CH³⁵). The binary mixture of 2:3 POPC/
 182 SM has an actual molecular area that is larger than its ideal and
 183 shows no condensation. The differences between the CH-induced
 184 condensation of 18:0 SM and POPC arise from the unsaturated
 185 acyl chain of POPC that reduces the efficiency of the molecular
 186 packing and leads to a higher molecular area for both its pure
 187 and binary mixtures. Interestingly, the ternary mixture behaves
 188 more like the binary phospholipid/CH mixtures with the addition
 189 of the second phospholipid (percent difference of -5% for 4:3
 190 POPC/CH + 47% SM and 4% for 2:1 SM/CH + 30% POPC),
 191 rather than the binary phospholipid mixture plus CH (percent
 192 difference of -20%).

193 The ternary mixture contains a saturated lipid (SM), an
 194 unsaturated lipid (POPC), and CH. Saturated lipids are more
 195 readily condensed by CH and will therefore be more prevalent
 196 in the CH-rich condensed phase,¹² whereas unsaturated lipids
 197 have a more limited condensation due to rigid double bonds.
 198 TOF-SIMS allows for the visualization of this within the ternary
 199 system and is evidenced in the following sections.

200 **TOF-SIMS Identifies Each Lipid in a Mixture.** Using TOF-
 201 SIMS, all lipids are identified within each of the monolayer
 202 systems using mass fragments unique to each lipid. The mass
 203 spectra for the pure lipids are presented in Figure 3. The molecular
 204 structures of each of the lipids, along with their corresponding
 205 unique positive ion SIMS fragments, are presented in Figure 4.
 206 The gold substrate is detected in each of the spectra (Au^+ at m/z
 207 197). The CH fragments are $[M - H]^+$ at m/z 385 and $[M -$
 208 $OH]^+$ at m/z 369. Although phosphocholine ($[C_5H_{15}NPO_4]^+$ at
 209 m/z 184) is a prevalent fragment, it arises from both POPC and
 210 18:0 SM and thus cannot be used to differentiate the location of
 211 one from the other. However, the protonated molecular ions, $[M$
 212 $+ H]^+$, are detected and used for both phospholipids: m/z 731
 213 for 18:0 SM and m/z 760 for POPC. Also, POPC headgroup

214 fragment $[C_8H_{19}NPO_4]^+$ at m/z 224 is unique to POPC because
 215 it includes a portion of the glycerol backbone. The sphingosine
 216 backbone fragment $[C_{17}H_{30}ON]^+$ at m/z 264 is a second fragment
 217 unique to 18:0 SM. Although not shown, all lipids were detected
 218 in each of the binary mixtures, and the ion images were found
 219 to be homogeneous with each lipid present throughout. The 16-
 220 mercaptohexadecanoic acid SAM is also observed in the mass
 221 spectra with most of its respective peaks below m/z 200. More
 222 importantly, none of the SAM peaks overlap with the lipid peaks
 223 of interest.²⁹

224 The mass spectrum of the ternary 30:47:23 POPC/SM/CH
 225 mixture is presented in Figure 5A. Each of the unique lipid
 226 fragments mentioned above is detected in this mixture. Although
 227 their intensities are low, the 18:0 SM peaks ($[M + H]^+$ at m/z
 228 731 and $[C_8H_{19}NPO_4]^+$ at m/z 224) are detected. The lower
 229 intensity in the upper part of the images is likely due to a slight
 230 tilt of the sample in the instrument. The tilt is caused by mounting
 231 the sample onto a copper stage for SIMS analysis after it is made.
 232 Thus, it does not affect the domain segregation that occurs at the
 233 air–water interface before the sample is transferred onto the
 234 substrate and subsequently mounted onto the copper stage. The
 235 quantitative examination presented later included samples with
 236 and without tilt artifacts, and no statistical difference was seen
 237 between them. The SIMS image of samples without a tilt artifact
 238 is presented in Figure 1 of Supporting Information. Note that the
 239 total ion image (Figure 5B) and phosphocholine image (Figure
 240 5C) both hint at nearly circular domain formation in the slight
 241 variation of intensity across the surface. Most importantly, the
 242 addition of CH induces domain formation, and this will be more
 243 clearly evidenced in the next section.

244 **Sphingomyelin Localizes with Cholesterol, and POPC is**
 245 **Excluded.** The individual lipid localizations for the ternary
 246 mixture (shown in Figure 5A) are presented in Figure 6. The data
 247 clearly show multiple liquid phases and the location of each
 248 lipid. The size and shape of the CH domains are similar to those

(35) Smaby, J. M.; Momsen, M.; Kulkarni, V. S.; Brown, R. E. *Biochemistry* 1996, 35, 5696–5704.

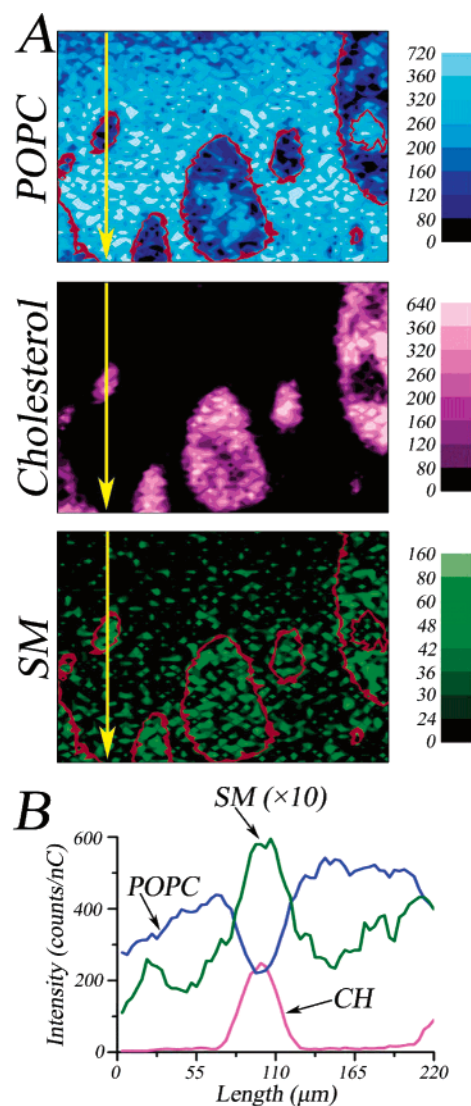


Figure 6. (A) Lipid molecular ion intensity mappings for 30:47:23 POPC/18:0 SM/CH. The +SIMS total ion image is presented in Figure 3D. The POPC signal ($[M + H]^+$ at m/z 760 and $[C_8H_{19}NPO_4]^+$ at m/z 224) is represented in blue, the CH signal ($[M - H]^+$ at m/z 385 and $[M - OH]^+$ at m/z 369) is represented in pink, and the SM signal ($[M + H]^+$ at m/z 731 and $[C_{17}H_{30}ON]^+$ at m/z 264) is represented in green. The outlines of the cholesterol domains (red) in the POPC and SM images are shown for emphasis. The ion intensity scales are in counts/nC, and the field of view is $320 \mu\text{m} \times 220 \mu\text{m}$. (B) Ion intensity line scan for each of the lipid ion maps. The region of the line scan is indicated by the yellow arrow in A.

249 shown in previous work,⁹ with the central domain being
 250 approximately $90 \mu\text{m}$ in diameter. The ion signal for POPC is
 251 lower in the CH-rich phase, indicating that it is excluded, whereas
 252 the ion signal for SM is most intense in the regions containing
 253 CH. The localization of SM is less clear as a result of the overall
 254 lower ion signal of the SM fragments. An intensity line scan
 255 through the ion images (Figure 6B) shows the varying intensity
 256 of each lipid signal. The CH ion yield begins at zero counts and
 257 rises to show a single $\sim 40 \mu\text{m}$ CH domain. The ion signal for
 258 POPC begins high but falls sharply at the CH domain, indicating
 259 that it is excluded from this densely packed region. In contrast,
 260 the ion yield for SM varies in a spatial pattern similar to the ion
 261 signal of CH. From Figure 6B, the relative yield of each
 262 phospholipid in the CH-rich phase versus that in the CH-poor
 263 phase is 2:1 for SM and 1:2 for POPC. Thus, SM is localized

264 within the CH-rich phase. Four samples of the ternary mixture
 265 were made and analyzed, and similar results were obtained for
 266 each.

Lipid Segregation Not Complete. The degree of lipid
 267 segregation between phases is evident in Figure 6. The line scan
 268 in Figure 6B shows that CH has nearly complete segregation
 269 into circular micrometer-size domains; however, neither the POPC
 270 nor SM signals fall to zero in the phase where they are least
 271 concentrated, thus neither SM nor POPC is completely segregated
 272 from these phases. This is a significant observation and
 273 demonstrates a unique capability of TOF-SIMS imaging. The
 274 lack of complete lipid segregation further illustrates the
 275 complexity of the lipid interactions. Strong physicochemical
 276 interactions between SM and CH should draw these lipids closer
 277 together and increase their segregation from POPC. The
 278 phospholipids in this system are not drawn completely into one
 279 phase or the other but rather are more prevalent in the phases
 280 where interactions are more favorable. Hence the structure of
 281 SM does not lead to interactions with CH that are dominant
 282 enough to entice complete segregation.

Quantification of Lipid Content. It would be valuable to
 284 extract quantitative compositional information directly from the
 285 images shown in Figure 6. For mass spectrometry experiments
 286 in general^{36–39} and for SIMS experiments in particular,^{30,40,41}
 287 ion signal intensity is not typically proportional to concentration
 288 because of what are generally referred to as matrix effects. For
 289 the system studied here, for example, it has been shown that
 290 when CH is co-localized with phosphocholine–phospholipids,
 291 proton transfer can increase the intensity of phosphocholine
 292 ($[C_5H_{15}NPO_4]^+$ at m/z 184).³⁰ However, there are strategies that
 293 can be employed to take into account these matrix effects and
 294 provide at least an estimate of the composition of lipids inside
 295 and outside the CH domains shown in Figure 6. Our approach
 296 is to calculate a relative sensitivity factor (*RSF*) for each of the
 297 three lipid components in the LB films. *RSF* is used most
 298 commonly in the elemental analysis of doped materials.^{42–44}
 299 When the matrix elemental concentration is constant, then *RSF*
 300 is defined by
 301

$$RSF_x = \frac{I_x}{C_x I_M} \quad (3)$$

where RSF_x is the relative sensitivity factor for component x ; C_x
 302 is the concentration of component x ; I_M is the secondary ion
 303 intensity of the matrix reference ion; and I_x is the secondary ion
 304 intensity for the relevant ion of component x . A number of
 305 different reference ions, including Au^+ and several major peaks
 306 from 16-mercaptohexadecanoic acid SAM, were examined. We
 307 finally chose Au^+ at m/z 197 because its intensity is most constant
 308 from sample to sample. The values for the single-component
 309 lipid films are given in Table 2. Note that the *RSF* value for CH
 310 is more than 50 times larger than for SM and 6.6 times larger
 311 than for POPC.
 312

(36) Schiller, J.; Arnhold, J.; Benard, S.; Müller, M.; Reichl, S.; Arnold, K. *Anal. Biochem.* **1999**, *267*, 46–56.

(37) Benard, S.; Arnhold, J.; Lehnert, M.; Schiller, J.; Arnold, K. *Chem. Phys. Lipids* **1999**, *100*, 115–125.

(38) Petković, M.; Schiller, J.; Müller, M.; Benard, S.; Reichl, S.; Arnold, K.; Arnhold, J. *Anal. Biochem.* **2001**, *289*, 202–216.

(39) Schiller, J.; Zschörnig, O.; Petković, M.; Müller, M.; Arnhold, J.; Arnolck, K. *J. Lipid Res.* **2001**, *42*, 1501–1508.

(40) Cannon, D. M., Jr.; Winograd, N.; Ewing, A. G. *Annu. Rev. Biophys. Biomol. Struct.* **2000**, *29*, 39–263.

(41) Roddy, T. P.; Cannon, D. M., Jr.; Ostrowski, S. G.; Winograd, N.; Ewing, A. G. *Anal. Chem.* **2003**, *75*, 4087–4094.

(42) Wilson, R. G. *J. Appl. Phys.* **1998**, *63*, 5122–5125.

(43) Novak, S. W.; Wilson, R. G. *J. Appl. Phys.* **1991**, *69*, 463–465.

(44) Wilson, R. G.; Novak, S. W. *J. Appl. Phys.* **1991**, *69*, 466–474.

Table 2. Relative Sensitivity Factors (RSF) for Each of the Lipid Components in the One-, Two-, and Three-Component Lipid LB Films^a.

| sample composition | Relative Sensitivity Factor (RSF) | | |
|-------------------------|--|--|--|
| | CH | SM | POPC |
| | [M - OH] ⁺ (<i>m/z</i> 369) | [C ₁₇ H ₃₀ ON] ⁺ (<i>m/z</i> 264) | [C ₈ H ₁₉ NPO ₄] ⁺ (<i>m/z</i> 224) |
| cholesterol (CH) | 0.72 ± 0.1 | | |
| 18:0 sphingomyelin (SM) | | 0.013 ± 0.001 | |
| POPC | | | 0.11 ± 0.005 |
| 2:3 POPC/SM | | 0.026 ± 0.001 | 0.17 ± 0.01 |
| 4:3 POPC/CH | 0.34 ± 0.002 | | 0.13 ± 0.01 |
| 2:1 SM/CH | 0.38 ± 0.005 | 0.23 ± 0.001 | |
| 30:47:23 POPC/SM/CH | 0.31 ± 0.003 | 0.021 ± 0.002 | 0.21 ± 0.02 |

^a All the calculations included at least three measurements of different areas in one or two samples.

The magnitude of matrix effects can be discerned by calculating the *RSF* values for all combinations of binary components, that is, 2:3 POPC/SM, 4:3 POPC/CH, and 2:1 SM/CH for conditions where there is no observable domain formation. The molar ratios of the lipid components in these binary systems are the same as the ratios utilized in the ternary system. For the three-component system, the *RSF* values may be obtained directly from a region of the monolayer that represents the macroscopic stoichiometry. These calculations assume that the concentrations reported for the two- and three-component systems are identical to the concentrations of the lipid mixtures applied to the LB trough. These values are also reported in Table 2. Note that the *RSF* values for CH are lower by about a factor of 2 and the *RSF* values for SM are higher by about a factor of 2. These changes are consistent with the proton-transfer mechanism noted above.

The two-component *RSF* values have been used to estimate the average concentration of each component in a three-component film. The *RSF* values of the two-component mixtures were averaged and applied to the signal intensities measured for the three-component mass spectrum. These results are shown in Table 3. The agreement between the expected values and the calculated values provides a sense of the reliability of the numbers. Similarly, using the *RSF* values calculated from the two- and three-component films, it is possible to estimate the molar concentrations of each species inside and outside the CH domains shown in Figure 6. Two methods were employed. In the first method (a), the two-component *RSF* values were applied to the measured ion intensity inside and outside a CH domain shown in Figure 6. In the second method (b), the *RSF* values of the three-component film were applied directly to these secondary

Table 3. Concentration of Each of the Lipid Components within and outside the Cholesterol Domains of Figure 5^a

| 30/47/23 POPC/SM/CH | CH | | 18:0 (SM) | | POPC | |
|------------------------|--|--------|--|--------|--|--------|
| | [M - OH] ⁺ (<i>m/z</i> 369) | | [C ₁₇ H ₃₀ ON] ⁺ (<i>m/z</i> 264) | | [C ₈ H ₁₉ NPO ₄] ⁺ (<i>m/z</i> 224) | |
| | a | b | a | b | a | b |
| Concentration (%) | | | | | | |
| entire sample | 19 ± 2 | | 43 ± 2 | | 38 ± 2 | |
| within CH domains | 20 ± 2 | 21 ± 2 | 61 ± 2 | 65 ± 6 | 19 ± 1 | 14 ± 1 |
| outside CH domains | 0 | 0 | 20 ± 1 | 31 ± 3 | 80 ± 4 | 69 ± 7 |

^a The concentration was determined in (a) using the *RSF* values for the two-component systems and in (b) using the *RSF* values for the three-component system. Note that the error in concentration arises from the *RSF* value used in the calculation.

ion intensities. The results are shown in Table 3. The magnitude of the numbers certainly suggests that SM is more concentrated in the CH domains and that POPC is presently largely outside the CH domain, as is evident from an inspection of Figure 6.

Implications

The location and relative amounts of each of the lipid components in a mixture of immiscible liquid phases have been determined using TOF-SIMS imaging without the need for labels or markers. The ternary mixture of 30:47:23 POPC/18:0 SM/CH produces coexisting liquid phases in which the SM localizes with CH while POPC is antilocalized with CH. However, the degree of lipid segregation is not complete, and further investigation of this phenomenon could help explain how lipid rafts on the order of a few molecules combine to form larger rafts in the cellular membrane. These results show the promise that TOF-SIMS imaging holds for resolving co-localized lipids and lipids present at varying concentrations.

Acknowledgment. Financial support was obtained from the National Institutes of Health and the National Science Foundation. We acknowledge Dr. David L. Allara and his research group for gold deposition and the use of their ellipsometer.

Supporting Information Available: Lipid molecular ion intensity mappings for another sample of 30:47:23 POPC/18:0 SM/CH without the sample tilt artifact. This material is available free of charge via the Internet at <http://pubs.acs.org>.

343
344
345
346
347
348
349
350
351
352
353
354
355
356
357
358
359
360
361
362
363
364
365
366
367
368